



The role of exponential asymptotics and complex singularities in self-similarity, transitions, and branch merging of nonlinear dynamics

S. Jonathan Chapman^a, Michael C. Dallaston^b, Serafim Kalliadasis^c, Philippe H. Trinh^{d,*}, Thomas P. Witelski^e

^a Mathematical Institute, Andrew Wiles Building, Woodstock Road, Oxford, Oxfordshire OX2 6GG, UK

^b School of Mathematical Sciences, Queensland University of Technology, Brisbane, QLD 4000, Australia

^c Department of Chemical Engineering, Imperial College London, London SW7 2AZ, United Kingdom

^d Department of Mathematical Sciences, University of Bath, Bath, Somerset BA7 7AY, UK

^e Department of Mathematics, Duke University, Box 90320, Durham, NC 27708-0320, USA

ARTICLE INFO

Article history:

Received 24 July 2022

Received in revised form 21 April 2023

Accepted 23 May 2023

Available online 21 June 2023

Communicated by Dmitry Pelinovsky

Keywords:

Exponential asymptotics

Thin-film flows

Similarity solutions

Fluid dynamics

Complex analysis

ABSTRACT

We study a prototypical example in nonlinear dynamics where transition to self-similarity in a singular limit is fundamentally changed as a parameter is varied. Here, we focus on the complicated dynamics that occur in a generalised unstable thin-film equation that yields finite-time rupture. A parameter, n , is introduced to model more general disjoining pressures. For the standard case of van der Waals intermolecular forces, $n = 3$, it was previously established that a countably infinite number of self-similar solutions exist leading to rupture. Each solution can be indexed by a parameter, $\epsilon = \epsilon_1 > \epsilon_2 > \dots > 0$, and the prediction of the discrete set of solutions requires examination of terms beyond-all-orders in ϵ . However, recent numerical results have demonstrated the surprising complexity that exists for general values of n . In particular, the bifurcation structure of self-similar solutions now exhibits branch merging as n is varied. In this work, we shall present key ideas of how branch merging can be interpreted via exponential asymptotics.

Crown Copyright © 2023 Published by Elsevier B.V. This is an open access article under the CC BY license (<http://creativecommons.org/licenses/by/4.0/>).

1. Introduction

In the study of singularly perturbed boundary-value problems, it is common to encounter situations in which boundary conditions overdetermine or overconstrain the problem. Then, it may be that in the singularly perturbed limit, say $\epsilon \rightarrow 0$, a countably discrete set of solutions emerge, each solution indexed by a value of ϵ . Well-known examples arise in a number of areas such as models of dendritic crystal growth and viscous fingering. In such cases, the critical selection mechanism is determined by terms beyond-all-orders in ϵ , and techniques in exponential asymptotics are required for its resolution [1]. This theory indicates that across critical Stokes lines in the complex plane, exponentially-small contributions may switch-on or -off. These exponentially-small terms then play a key role in satisfying the boundary conditions. In this paper, we demonstrate a further complexity that arises in a problem related to the rupture of a thin film with generalised disjoining pressures. In this case, a key parameter in the differential equation can fundamentally alter the complex-plane structure, leading to branch merging (cf. Fig. 4).

Indeed, we may view the above scenario as a prototypical example in nonlinear dynamics and fluid motion, where transition to self-similarity in a singular limit is fundamentally changed as a parameter of the governing system is varied. Although this situation is quite ubiquitous, the mathematical approach we employ for its description, using exponential asymptotics or asymptotics beyond-all-orders, is compelling, powerful and seems to be universal.

Consider a two-dimensional thin viscous film of height $h(x, t)$, placed on a planar horizontal solid substrate. The film is subject to surface tension effects and long-range attractive intermolecular van der Waals forces. After appropriate non-dimensionalisation, the governing differential equation is then given by (cf. eqn (1.1) in [2])

$$\frac{\partial h}{\partial t} = -\frac{\partial}{\partial x} \left(h^3 \frac{\partial^3 h}{\partial x^3} \right) - \frac{\partial}{\partial x} \left(\frac{1}{h} \frac{\partial h}{\partial x} \right), \quad (1)$$

with h being the film thickness, x a spatial coordinate, and t being time. This evolution equation will be accompanied by appropriate initial and boundary conditions. The first term in its right-hand side describes surface-tension-driven flow, while the second term gives contributions due to van der Waals forces. Generically, solutions of (1) present an unstable interface that ruptures in finite time. Near the critical time, $t = t_c$, and point, $x = x_c$ of

* Corresponding author.

E-mail address: p.trinh@bath.ac.uk (P.H. Trinh).

rupture, it was shown by Zhang & Lister [3] that for $t < t_c$, there exists similarity solutions of the form

$$h(x, t) = \tau^{1/5} H(\eta) \quad \text{with } \eta = \frac{x - x_c}{\tau^{2/5}}, \quad (2)$$

with $\tau = t_c - t$. Moreover, there exists a discrete countably infinite number of solutions, say $H = H_n(\eta)$, where each solution is distinguished by a different far-field condition $H_n \sim \epsilon_n^{2/5} |\eta|^{1/2}$ as $\eta \rightarrow \pm\infty$ (see e.g. Zhang & Lister [3] and Witelski & Bernoff [4]). Self-similar solutions are obtained from a nonlinear boundary-value problem yielding a set of discrete eigenvalues, $\epsilon_1 \approx 0.651$, $\epsilon_2 \approx 0.304$, $\epsilon_3 \approx 0.205$, ... In general, this is done numerically; however, analytical prediction in the limit of $\epsilon_n \rightarrow 0$ and $n \rightarrow \infty$ is possible using sophisticated techniques in exponential asymptotics [2]. A basic question that motivates this work is whether the above self-similar structure, and its limiting asymptotic analysis, is expected to be the same for general forms of the disjoining pressure, beyond the standard van der Waals forces, and hence for modifications of those corresponding terms in (1).

Adopting a wider view, consider some critical aspects of general behaviour of nonlinear dynamical systems. Such systems may depend crucially on the values of governing parameters, including exponents, within the systems. As parameters are varied, the transition that takes place from one set of behaviours to another, can be understood by tracking the branches of invariant solutions, such as steady states, periodic orbits, similarity solutions, and so forth. We are particularly interested in their bifurcation structures, and hence the changes in the number or stability of such invariant solutions.

One such transition is the change from universal self-similarity to the formation of complex iterated patterns. Iterated patterns are ubiquitous in a wide spectrum of natural phenomena, technological applications and art creations: from the dendritic structure of trees, river deltas and bio-morphology, to architecture and designer surfaces including jewellery, textiles, wallpaper and ceramics. Mathematically, iterated patterns may be appreciated in the context of fractal geometry, where they are constructed by design [5]. The complexity of iterated patterns is believed to lie at the heart of some of physics' deepest problems, such as turbulence. We note, for instance the seminal studies of Choptuik on scaling and universality in gravitational collapse [6] and Pumir and Siggia's discussion of chaotic self-similarity in the Euler equation [7]. In the context of nonlinear dynamics, iterated structures may arise as emergent phenomena, i.e. the result of cooperative phenomena between autonomously behaving elements: a group of elements creates a self-organising structure, which governs the individual micro-rules of a system and creates a new macro-structure.

Returning to (1), the form of the second order term due to the disjoining pressure can be expected to change subject to different physical conditions: the van der Waals interactions are typically induced-dipole-induced-dipole interactions and scale as r^{-6} with r the distance between two neighbouring molecules. Changing the liquid and/or solid substrate changes the type of interaction, e.g. the hydrogen bonding in water is a (fixed) dipole-dipole interaction scaling as r^{-4} . Such effects alter the disjoining pressure exponent, which determines the form of the second order term in (1). In this context, thin film rupture for a model with a generalised disjoining pressure,

$$\frac{\partial h}{\partial t} = -\frac{\partial}{\partial x} \left(h^3 \frac{\partial^3 h}{\partial x^3} \right) - \frac{\partial}{\partial x} \left(h^{2-n} \frac{\partial h}{\partial x} \right), \quad (3)$$

with $n > 0$ was considered recently by Dallaston et al. [8,9], who discovered that this equation can generate iterated structures of tremendous complexity. An illustration of the bifurcations in

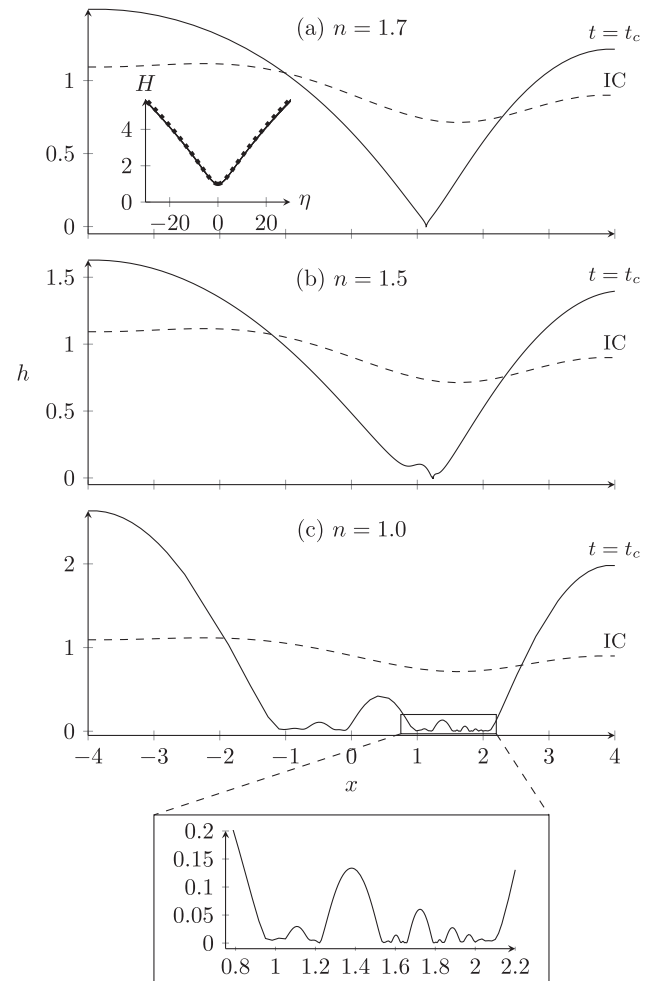


Fig. 1. Numerically computed solution profiles of Eq. (3) for different values of the exponent n , close to the critical time t_c at which $h = 0$ at a point, after which solutions cease to exist [9]. For (a) $n = 1.7$, the solution profiles collapse onto the similarity solution (a solution of (6), shown in the dotted line inset, in similarity coordinates η, H). For (b) $n = 1.5$, the solution profiles do not collapse onto a similarity solution (they can be shown to asymptote to a periodic, rather than steady, solution in the similarity coordinates), as no stable similarity solution exists for this parameter regime. For (c) $n = 1.0$ this behaviour is more pronounced, and detailed iterated patterns are produced.

this behaviour is shown in Fig. 1. The generative mechanism for the formation of iterative structures involves two characteristics: (i) the annihilation of universal similarity solutions via branch merging (i.e., fold bifurcations or turning points) as the exponent n varies; and (ii) the creation of branches of periodic orbits via Hopf bifurcations in a scaled coordinate system that correspond to discretely self-similar behaviour (where invariance occurs only at discrete times). The transition occurs over a small range of the n -parameter. The numerical studies in Refs. [8,9] do not categorise the complete bifurcation structure in this critical parameter regime, and the details of the transition are not yet fully understood. In this work we focus on the phenomenon of branch merging, and how it can be analysed with exponential asymptotics. The complete nature of the bifurcation structure requires full determination of the stability characteristics of the similarity solutions, which is beyond the scope of the methods described here.

What is particularly interesting is that within the context of thin-film fluid dynamics, the model in (3) has primarily been

examined for the prototypical case of $n = 3$, where the second term on the right-hand side corresponds to modelling the effects of van der Waals forces. It is interesting, though perhaps not wholly unexpected, that changes in the value of parameter n , and hence considering more generalised molecular laws (which are themselves only approximate), can have a significant effect on the structure of solutions.

1.1. A methodology using exponential asymptotics

We outline an exponential asymptotic methodology for describing the branch-merging of similarity solutions to (3). The equation is used as a paradigm example of this phenomenon and the methods described are anticipated to be widely applicable to other singularly perturbed problems. Branch-merging, for either similarity solutions or other invariant solutions, arises in many nonlinear systems, and the loss of invariant solutions will always have implications for the dynamics, and even long-time existence, of solutions in general. For example, branch-merging occurs in similarity solutions of viscous fingers in Hele-Shaw flow for sufficiently small surface tension [10,11], and the loss of stable solutions is expected to be the cause of tip splitting and side-branching phenomena in radially expanding bubbles (see Fig. 2).

One of the results from our work is to demonstrate that the above phenomena of branch merging, when studied in the context of a singular perturbation problem, can be explained by the asymptotic analysis of nonlinear eigenvalue problems where a countably infinite sequence of eigenvalues appears in the asymptotic limit.

As a foundational example and to fix ideas, consider the annihilation of real eigenvalues in non-Hermitian Hamiltonian eigenvalue problems arising in quantum mechanics [12]. Here, the time-independent solutions are governed by an ordinary differential equation (ODE), a Schrödinger eigenvalue problem for $\psi = \psi(x)$, e.g. from Bender & Boettcher [12],

$$-\frac{d^2\psi}{dx^2} + (ix)^{\epsilon}x^2\psi = E\psi,$$

and E is the eigenvalue. The wave function ψ must tend to zero in appropriate sectors of the complex x -plane. For $\epsilon > 0$, the eigenvalues $E = E_n(\epsilon)$ are real and form a countably infinite set, $E_0 < E_1 < E_2 < \dots$. However, as ϵ passes from positive to negative values, the branches of adjacent eigenvalues corresponding to, e.g. E_n and E_{n+1} , merge and for smaller values of ϵ , these eigenvalues are complex in nature. The challenge is to explain why this critical transition occurs at $\epsilon = 0$. Recently, methods similar to those described in this article have been successfully applied to such problems [13]. Let us note that mathematically, branch merging is likely to play a role in the prediction of Fujita-like exponents (critical values of exponents that separate regions where all solutions blow up in finite time, and regions where long-time existence of solutions is possible [14]) for higher-order partial differential equations (PDEs) such as (3), but also other thin-film problems, such as falling liquid films where the contribution from inertia is responsible for finite-time blow up [15].

Exponential asymptotic analysis is a tool that has enjoyed success in predicting the existence of discretely selected solutions for numerous linear and nonlinear systems in engineering and physics. We mention, for example, applications in wave and quantum mechanics [13,17,18], Saffman-Taylor viscous fingering [10,19–21], free-surface water waves [1,22,23], localised pattern formation [24], and vortex reconnection [25]. But also the study of the self-similar solutions of (3) in the case of $n = 3$ [2]. Such methods in exponential asymptotics apply when, in some limit (in this case corresponding to large branch number),

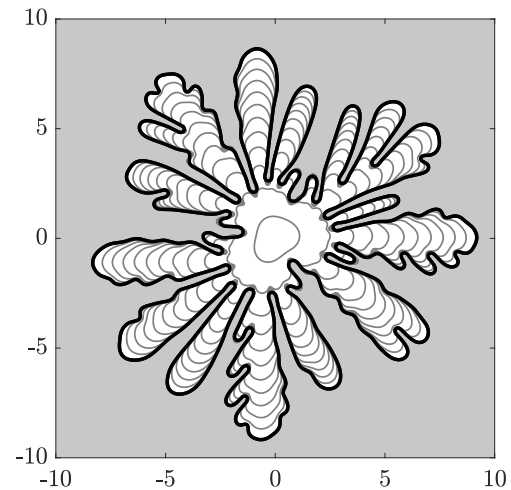


Fig. 2. Numerical solution of a growing bubble in a Hele-Shaw cell, demonstrating the phenomenon of tip-splitting and side-branching (from [16]). These instabilities are thought to result from the loss, via branch merging, of stable self-similar finger solutions [10,11].

the selection mechanism is due to exponentially small oscillatory terms that are missed in an algebraic asymptotic expansion. To understand how these terms arise and interact, the singularity structure of the early asymptotic orders is required in the complex plane. Indeed, one of the main contributions of this work is to emphasise the importance of such complex singularities on the bifurcation structures of the governing ODE or PDE.

Our overarching objective for this article is two-fold. Firstly, we shall extend the methodology presented in the work of Chapman et al. [2] for the study of self-similar rupture solutions of (3), there studied for $n = 3$, to the generalised values of n considered in the recent works of Dallaston et al. [8,9,26]. We will show that branch merging occurs for general n , and this can be anticipated by examining changes in the leading-order solutions in the complex plane. Secondly, we wish to explain these phenomena in a simplified fashion so that the theory is accessible to non-specialists in the area of asymptotic analysis (in contrast, e.g., to the full complexity of [2]). In addition to elucidating the behaviour of (3) as n decreases, we anticipate that the analysis presented in this work will be applicable to other nonlinear systems (self-similar or otherwise) that exhibit branch merging described above.

2. Physical and mathematical formulation

As we have already noted, physically, the evolution equation (3) may be used to describe the dynamics of a two-dimensional thin viscous liquid film over a planar horizontal solid substrate. Thin films are of great interest in technological and scientific applications [27–29], and despite occurring on a wide variety of spatial scales, many thin-film models fit into the same framework, being described (ideally or asymptotically) by (3). The fourth-order surface tension terms in the right-hand side are always stabilising; in contrast the second-order terms are always destabilising and are derived from a number of different physical effects, with the exponent n depending on the particular effect being modelled. Some of the destabilising effects that fit into this framework are attractive van der Waals forces ($n = 3$) which we have already discussed, including intermolecular forces ($n = 0$ to $n = 4$) [30], thermocapillary instability ($n = 0$) [31,32],

Rayleigh–Taylor instability [33] and evaporative vapour recoil ($n = -1$) [34].

A question of both practical and mathematical concern is whether the film thickness, h , will reach zero at a finite time at any point: in physical terms, whether the film ruptures. Practically, if the film does rupture, additional physical effects must be included in the model to describe post-rupture dewetting. Rupture and dewetting are often undesirable; for instance, in heat transfer applications, this results in the dramatic reduction of heat transfer that can lead to local overheating and subsequent material damage. From a mathematical perspective, rupture is a form of finite-time blowup that prevents long time existence of solutions to (3).

To find rupture solutions to (3), we define the similarity coordinate variable, η , via

$$h(x, t) = \tau^\alpha H(\eta) \quad \text{with } \eta = \left(\frac{x - x_c}{\tau^\beta} \right), \quad (4)$$

with $\tau \equiv t_c - t$. As noted by [8], for rupture solutions to exist, we must assume $n > 1/2$, with

$$\alpha = \frac{1}{2n-1} \quad \text{and} \quad \beta = \frac{n+1}{4n-2}. \quad (5)$$

Then self-similar solutions are governed by the ODE

$$-\frac{d}{d\eta} \left(H^3 \frac{d^3 H}{d\eta^3} + H^{2-n} \frac{dH}{d\eta} \right) = -\alpha H + \beta \eta \frac{dH}{d\eta}. \quad (6)$$

Because rupturing is a localised process, at any fixed point, x , bounded away from x_c , the evolution of the profile remains essentially unaffected by the singularity as $t \rightarrow t_c$. Consequently, this yields a necessary far-field Robin boundary condition for self-similar solutions determining them to have the form,

$$H(\eta) \sim C|\eta|^{\alpha/\beta} \quad \text{as } |\eta| \rightarrow \infty. \quad (7)$$

Following [2], we shall assume that solutions are symmetric and hence solve on the domain $0 \leq \eta < \infty$ with symmetry conditions $H'(0) = 0 = H'''(0)$ (the existence, and instability, of asymmetric similarity solutions is explored in [26]). Moreover we scale the far-field constant, C , in (7) out, under the further transformations of

$$H(\eta) = C^a \phi(z) \quad \text{and} \quad \eta = C^b z, \quad (8)$$

with $a = 2\beta$ and $b = (2-n)\beta$. We now define ϵ such that

$$C = \epsilon^{2/(3a-4b)} = \epsilon^{2/(n+1)}. \quad (9)$$

Substitution into (6) provides the governing equation for the similarity profile, $\phi(z)$, given by

$$-\frac{d}{dz} (\epsilon^2 \phi^3 \phi''' + \phi^{2-n} \phi') = -\alpha \phi + \beta z \phi', \quad (10a)$$

where henceforth, primes (') denote differentiation in z . In addition, we enforce symmetry and a far-field “stationarity” condition (cf. [3]),

$$\phi'(0) = 0 \quad \phi'''(0) = 0, \quad (10b)$$

$$\phi \sim z^{\alpha/\beta} \quad \text{as } z \rightarrow \infty, \quad (10c)$$

and hence study only symmetric solutions on $z \in [0, \infty)$. Note that the re-scalings in (8) allow the far-field condition to be normalised, while the definition of $\epsilon > 0$ in (9) is introduced so that the singularly perturbed scaling in (10a) [with the leading ϵ^2] renders the subsequent analysis more convenient. As a check, if $n = 3$, $a = 4/5$ and $b = -2/5$ in (8), and furthermore, $C = \epsilon^{1/2}$, matching the van der Waals scaling chosen in [2].

As we shall see in Section 3, a WKB analysis of (10c) in the limit of $z \rightarrow \infty$ reveals that the single far-field conditions

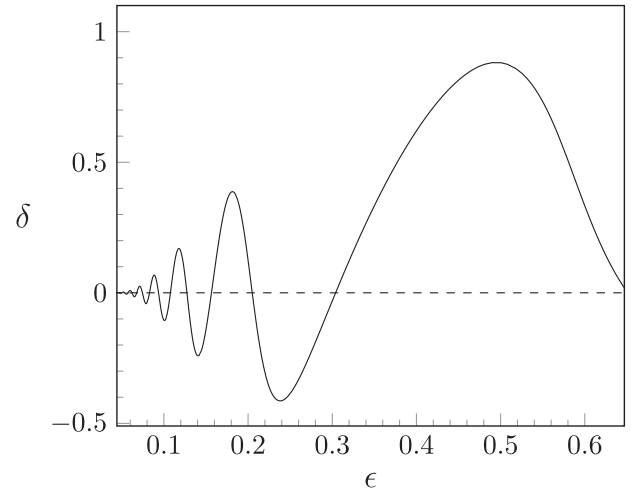


Fig. 3. In order to solve (10), we introduce the artificial parameter $\delta = \phi'''(0)$, and seek solutions for a given ϵ . The roots, where $\delta = 0$, then correspond to solutions to (10). The above graph shows $\delta(\epsilon)$ for the case of $n = 3$.

above applies three conditions on the solution. Then in combination with the two conditions (10b) at the origin, the five boundary conditions over-constrain the fourth-order PDE (10a). Consequently, we may expect solutions only at specific values of ϵ , which we now refer to as an eigenvalue.

Numerical solutions to the system (10) are computed using the schemes described e.g. in [8,9,35]. The basic procedure is summarised as follows. First, we start with the stable known profiles (such as the case $n = 3$). Then, for general $n > 1/2$, we treat the second boundary condition in (10b) as a shooting condition $\phi'''(0) = \delta$, and solve for solutions within a range of decreasing ϵ values. Once this is done, the curve $\delta = \delta(\epsilon)$ is established, such as the one in Fig. 3. Evidently the curve oscillates around 0, and every intersection with the dashed line corresponds to a discretely selected solution, where $\phi'''(0) = 0$.

Thus, at each value of n , we obtain a set of discrete eigenvalues. For sufficiently large n they are of the form $\epsilon_1(n) > \epsilon_2(n) > \epsilon_3(n) > \dots > 0$. As we have already hinted in the Introduction, we observe the merging of successive pairs of branches as n decreases, with the first merge occurring at $n \approx 1.5$, and successive ones at smaller values of n as the branch number increases (or equivalently, ϵ decreases). The goal now is to produce an asymptotic theory of this structure, valid as $\epsilon \rightarrow 0$.

3. The existence of exponentially small terms

It is possible to obtain some forewarning of the difficulties to come. The governing equation (10a) is a fourth-order problem and hence at least four boundary conditions are required. The symmetry conditions about the origin in (10b) provide two, but in fact, the requirement in (10c) that $\phi \sim z^{\alpha/\beta}$ as $z \rightarrow \infty$ is equivalent to an additional three independent constraints on the differential equation, a total of five conditions as already highlighted in Section 2. To make this latter result more transparent, let us expand ϕ in the limit $z \rightarrow \infty$. From (10a), it can be verified that ϕ can be written as an algebraic series in inverse powers of $z^{1/\beta}$, along with three exponential corrections, as given by

$$\phi \sim z^{\alpha/\beta} \left[1 + \frac{\tilde{a}_1}{z^{1/\beta}} + O\left(\frac{1}{z^{2/\beta}}\right) \right] + C_1 \phi_{\text{wkb},1} + C_2 \phi_{\text{wkb},2} + C_3 \phi_{\text{wkb},3}, \quad (11)$$

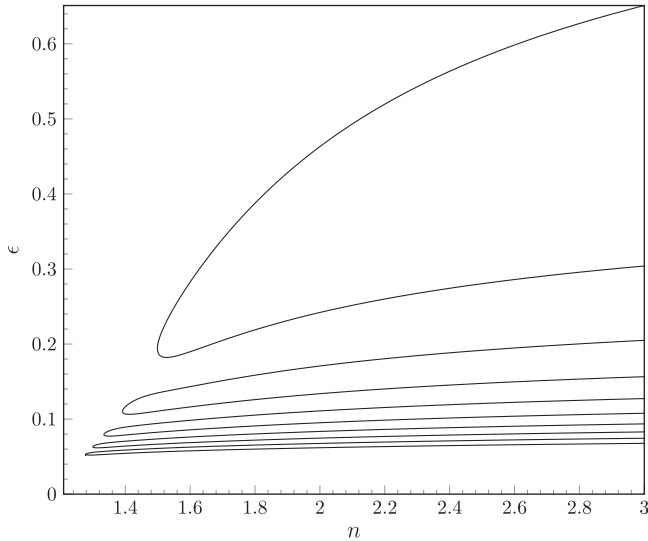


Fig. 4. At a fixed value of the disjoining pressure parameter, n , discrete sequences of solutions are found, each indexed by $\epsilon = \epsilon_m$. The first ten solution branches are shown. As n decreases, branches merge in pairs. Note that there are further solutions branches (not shown) that exist for smaller values of ϵ ; these are challenging to compute but the reader may compare with the asymptotic predictions in Fig. 9.

where we have chosen the leading coefficient to satisfy the boundary condition (10c), and \tilde{a}_k for $k = 1, 2, 3, \dots$ and C_i , $i = 1, 2, 3$ are complex-valued constants dependent on ϵ .

Next, substituting (11) into (10a), we see that in the far-field limit, the three terms on the right hand-side of (11) are approximated by a WKB approximation (see e.g. [36]):

$$\phi_{\text{wkb},k} \sim \frac{(\text{const.})\epsilon^{4/3}z^{-\frac{2}{3}\frac{n-5}{n+1}}}{B_k^2} \exp \left[\frac{B_k}{\epsilon^{2/3}\mu} z^\mu + \left(\frac{1}{3B_k\epsilon^{4/3}\mu} \right) z^{-\mu} + o(z^{-\mu}) \right], \quad (12)$$

where

$$B_k = \beta^{1/3} \exp[\pi i(2k+1)/3] \quad \text{and} \quad \mu = \frac{2}{3} \left(\frac{2n-1}{n+1} \right). \quad (13)$$

Thus, in order to impose the behavioural condition of $\phi \sim z^{\alpha/\beta}$ as $z \rightarrow \infty$ in (10c), we require that the coefficients of the two oscillatory modes in (11) are zero ($C_2 = 0 = C_3$). In combination with the two conditions at the origin, this yields a total of five boundary conditions for the differential equation (10a) and hence the problem is overdetermined. In connection with similar problems [2,25], it would be expected that solutions are valid only at specific values of ϵ , say, corresponding to a discrete countable set,

$$\epsilon_1(n) > \epsilon_2(n) > \dots > \epsilon_m(n) > \dots > 0, \quad (14)$$

where each distinct eigenvalue is dependent on the choice of disjoining parameter, n .

As it stands, however, the far-field expansion in (11) and exponential forms (12) are insufficient for determining the selection of eigenvalues ϵ_m . Indeed, we require knowledge of the exponential switchings throughout the real line in z (and not only the behaviour as $z \rightarrow \infty$), and most specifically at the origin where the additional symmetry conditions hold. Moreover, on the basis of the numerical results, we know that (14) does not describe the branch merging that manifests for sufficiently small n .

4. A brief explanation of the key result

Following the methodology in Chapman et al. [2] the mathematics used to resolve the generalised rupture problem turns out to be quite involved. However, the key ideas are comparatively easier to explain. Here, we aim to provide a simple explanation of why the branches in Fig. 4 merge.

We shall begin by discussing the generic occurrence of exponentially-small terms in singularly perturbed problems. The form of the ODE in (10a) suggests that we write the solution, ϕ , in terms of a regular series expansion in powers of ϵ , i.e.

$$\phi(z) \sim \sum_{m=0}^{\infty} \epsilon^m \phi_m(z). \quad (15)$$

It can be confirmed that the numerical solution follows the leading-order approximation, $\phi \sim \phi_0$, along the real z -axis. However, singularities in the analytic continuation of ϕ_0 cause the above series to diverge as $m \rightarrow \infty$, and hence the series should be truncated in practice. It is then the subsequent analysis of the remainder of the truncated series that provides key elements determining the selection mechanism for ϵ .

Hence, we optimally truncate (15), and write

$$\phi(z) = \sum_{m=0}^{N-1} \epsilon^m \phi_m(z) + R_N(z), \quad (16)$$

for N to be specified and seek an equation for the remainder, R_N . When substituted into (30a), this yields a linear equation for the remainder,

$$\mathcal{L}R_N \sim -\epsilon^{2N} \frac{d}{dz} (\phi_0^3 \phi_{N-1}'''). \quad (17a)$$

where we have defined the linear operator

$$\mathcal{L}R_N \equiv \left[\epsilon^2 \phi_0^3 \right] R_N'''' + \left[3\epsilon^2 \phi_0^2 \phi_0' \right] R_N''' + \left[\phi_0^{2-n} \right] R_N'' + \left[2(2-n)\phi_0^{1-n}\phi_0' + (2-n)\phi_0^{1-n}\phi_1 + \beta z \right] R_N'. \quad (17b)$$

As the remainder is assumed to be small, we have ignored nonlinear contributions in R_N . Eq. (17a) indicates that if the truncation parameter, N , is chosen arbitrarily, then the error is only algebraically small, and of the order of the first neglected term, $\mathcal{O}(\epsilon^{2N})$. However if N is chosen optimally, then R_N is exponentially small in ϵ [37,38]. We then wish to consider the necessary boundary conditions of (10) when applied to R_N .

With exponential smallness in mind, we may now consider a generic WKB ansatz for R_N ; by substitution and consideration of $\epsilon \rightarrow 0$, we find that the homogeneous equation, $\mathcal{L}R_N = 0$, is satisfied via

$$R_N \sim A(z)e^{-\chi(z)/\epsilon}, \quad (18)$$

where the key *singulant* function, χ , is found to be

$$\chi(z) = \pm i \int_{\sigma}^z K(t) dt \quad \text{with} \quad K(t) = \frac{1}{[\phi_0(t)]^{(n+1)/2}}. \quad (19)$$

For convenience of later analysis, the origin of integration, σ , in (19), is often – but not necessarily always – set to the singularities in the analytic continuation of the early asymptotic orders (e.g. ϕ_0). The chosen sign, \pm , can be determined by the requirement that $e^{-\chi/\epsilon}$ is exponentially small on the real axis. Similarly, by consideration of the next order terms in ϵ , a (transport) equation can be derived for the prefactor, $A(z)$, appearing in (18).

Returning now to the inhomogeneous equation for the remainder (17a), we may express the leading-order solution as $R_N(z) \sim S(z; \epsilon)A(z)e^{-\chi(z)/\epsilon}$, where S is the *Stokes switching factor*,

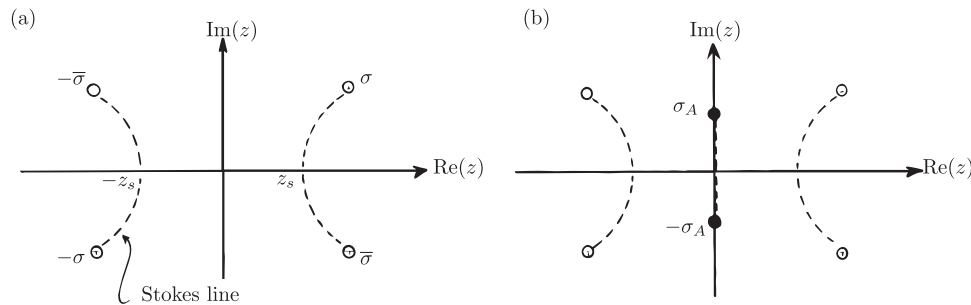


Fig. 5. (a) Illustration of Stokes line configuration for $n > n^* = 5/3$; (b) Illustration of Stokes line configuration for $n < n^*$. In situation (a) a localised oscillation exists in $[-z_s, z_s]$, in the region on the real axis between Stokes lines (dashed); this governs a selection mechanism on the eigenvalue, ϵ . In situation (b), additional singularities appear on the imaginary axis, σ_A and $-\sigma_A$, and now an additional central Stokes line (dashed) appears.

to be found from analysis. Following the Stokes-line smoothing procedures of [1,37,38], two key results emerge. The first is that there exists special curves (*Stokes lines*) in the complex plane, across which S smoothly switches-on from zero to a non-zero value. This is known as the *Stokes phenomenon*.

Notice that from the governing differential equation (10), the solution, ϕ , is real on the real z -axis. Thus, by the Schwarz reflection principle, we expect complex-conjugated Stokes lines generated in addition. Together, this implies that along the real z -axis, the remainder must include contributions of the form

$$\phi_{\text{exp}} \sim S(z; \epsilon) A(z) e^{-\chi(z)/\epsilon} + \text{c.c.} \quad (20)$$

Once the complex-valued functions of S , A , and χ are inserted, the above yields a real-valued oscillation on the real z -axis. If $\text{Re } \chi > 0$, which must be the case for satisfaction of boundary conditions, the oscillation is exponentially small.

Summarising, we have just described the generic process upon which exponentially-small terms switch on when the base expansion (15) is analytically continued. This switching across Stokes lines, we may write as

$$[\phi_0 + \epsilon^2 \phi_1 + \dots] \mapsto [\phi_0 + \epsilon^2 \phi_1 + \dots] + \phi_{\text{exp}}. \quad (21)$$

The above switching, involving the exponential (20), is quite a generic process associated with general divergent series in singularly perturbed differential equations.

We illustrate, in Fig. 5, how a contribution such as (20) can determine a selection process such as (14). Moreover, we shall see how this process can suddenly change, dependent on values of n . Firstly, in the illustration of Fig. 5(a), two Stokes lines (or curves) are shown in the complex z -plane. Each curve originates from and terminates at one of four singularities $\{\pm\sigma, \pm\bar{\sigma}\}$. The physical rupture solution is evaluated along the real axis, and we consider an analytic continuation procedure that begins from $-\infty$ and tends to $+\infty$ along the real axis.

As (15) is analytically continued across the point marked $z = -z_s$ in the figure, a term of the form (20) is switched on. A similar switching occurs across the point $z = +z_s$, producing a similar contribution (20). In order to satisfy the symmetry boundary conditions, what has been switched-on at $-z_s$ must be switched off at $+z_s$. This essentially results in a localised oscillatory interval in $[-z_s, z_s]$ and, with some work, provides a condition on the possible values of ϵ , dependent on the particular components of (20) such as $\chi(z)$ and $A(z)$. For the thin-film rupture problem, the situation in Fig. 5(a) is essentially what occurs when the general disjoining parameter and the countably infinite set of (14) is derived. As we shall explain, this setup occurs for $n > n^*$ where this critical value, $n^* = 5/3$ as $\epsilon \rightarrow 0$. In particular, this is the situation of the $n = 3$ case studied in [2].

However, if $n < n^* = 5/3$, the singularity structure of the associated problem changes and what results is a Stokes

line structure similar to the one illustrated in Fig. 5(b). In this case, an additional Stokes line appears along the imaginary axis between singularities σ_A and $\bar{\sigma}_A$ that causes an extra switching-on of the exponential term (20). However, unlike the arrangement shown in Fig. 5(a), there is no mechanism for turning off this particular exponentially-small oscillation as $|z| \rightarrow \infty$. At the point it is introduced, the additional oscillation is exponentially subdominant to the former localised oscillation; however, as n decreases the two contributions exchange in magnitude and for n sufficiently small (we show in Section 7 this to be around n less than ≈ 1.25), the latter invalidates the boundary condition (10c). The conclusion is that, for sufficiently small n , as $\epsilon \rightarrow 0$, there is no way to satisfy the required boundary conditions and solutions of the assumed type do not exist. This is essentially what causes the turning points in the bifurcation curves of Fig. 4 for smaller values of n .

Now, the task is to derive the particular exponentials (20) that govern the two cases illustrated in Fig. 5. The case of the symmetric arrangement yielding localised oscillations is described in Section 5, and the case of the asymmetric arrangement is described in Section 6.

5. Generation of the localised oscillations from $z \gg 1$

For the general values of n studied in this work, the exponential switchings that occur for the classic van der Waals case ($n = 3$) continue to be present, and the associated formulae need only be modified for the values of n . In the previous section, we presented a simplified view of these switchings via Fig. 5(a). The situation is somewhat more complex: as explained in Sec. 6 of [2], there exists a peculiarity in the nonlinear form of the differential equation (10a) which effectively causes a boundary layer at large values of z . As it turns out, it is easier to derive the exponential switching for $z \gg 1$, for which the result is then matched to the form of (20) when $z = \mathcal{O}(1)$. Because the associated solutions are simplified in the far-field, this analysis involves the manipulation of Airy-type Stokes phenomena and Stokes lines (see e.g. [39]). We note that the required algebra is not insignificant, and we include certain key formulae in Appendix A and Appendix B; however for brevity of this article, the full derivations are withheld and will be presented in a forthcoming work.

Before proceeding, note that we may obtain evidence of the boundary layer at infinity by examining the WKB solution (12). Observe that the second term of the exponential argument is of the same order as the first when

$$z = \mathcal{O}(\epsilon^{-1/(3\mu)}) = \mathcal{O}(\epsilon^{-\frac{1}{2} \frac{n+1}{2n-1}}) = \mathcal{O}(\epsilon^{-\beta}). \quad (22)$$

Therefore, when z reaches the above threshold, the WKB solution breaks down and this is indicative of a further re-scaled region.

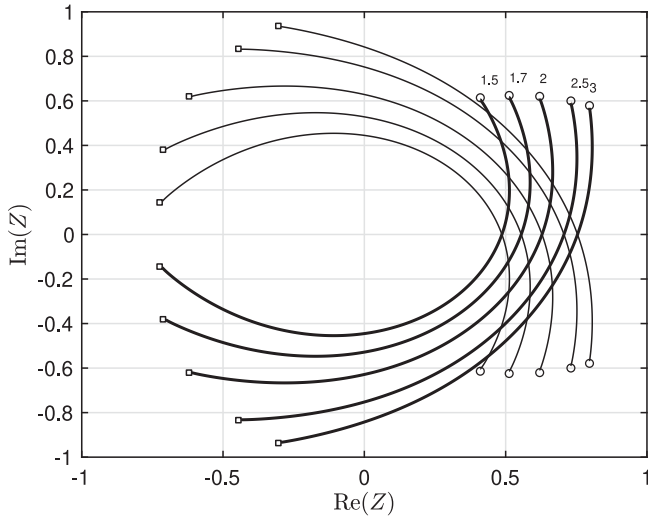


Fig. 6. This diagram shows the continuous shift of the Stokes lines as n decreases from $n = 3$ to $n = 1.5$ (corresponding numbers indicated). Circular nodes indicate turning points Z_0 (upper half-plane) and Z_{-1} (lower half-plane). Square nodes indicate turning points Z_2 (upper half-plane) and Z_{-2} (lower half-plane). The Stokes line where $A_1 e^{S_1/\epsilon}$ switches on $A_3 e^{S_3/\epsilon}$ is indicated thick and the Stokes line where $A_1 e^{S_1/\epsilon}$ switches on $A_2 e^{S_2/\epsilon}$ is indicated thin. This figure can be compared to Fig. 6 of [2], which only plots the case of $n = 3$.

Hence, we shall return to the original system (10), and set $z = Z/\epsilon^\beta$ and $\phi = (\epsilon^{-\beta})^{\alpha/\beta} f(Z)$. The governing equation is then

$$\frac{d}{dZ} \left(\epsilon^3 f^3 \frac{d^3 f}{dZ^3} + \epsilon f^{2-n} \frac{df}{dZ} \right) = \alpha f - \beta Z \frac{df}{dZ}. \quad (23)$$

The solution is sought as an asymptotic series in ϵ , plus a WKBJ correction:

$$f(Z) \sim [Z^{\alpha/\beta} + \epsilon f_1(Z) + \dots] + \tilde{A}(Z) e^{S(Z)/\epsilon}. \quad (24)$$

The above WKBJ ansatz is substituted into (23), and we obtain a cubic equation [given in (A.1)] for the derivative, $S'(Z)$, as well as a further transport equation for the prefactor, $\tilde{A}(Z)$. The three cubic roots then imply that the possible WKBJ behaviours are:

$$(\text{decaying WKBJ}) \tilde{A}_1(Z) e^{S_1(Z)/\epsilon} \quad (\text{oscillatory WKBJ}) \tilde{A}_{2,3}(Z) e^{S_{2,3}(Z)/\epsilon}, \quad (25)$$

where the classification of ‘decaying’ and ‘oscillatory’ applies along the real Z -axis. The above three modes are related to the three corresponding modes in the $z \rightarrow \infty$ expressions of (12). The exponential arguments, S_i for $i = 1, 2, 3$, are given by integrating (A.2).

Recall in the discussion regarding (12) that for $z \rightarrow +\infty$, the decaying mode corresponding to $\tilde{A}_1(Z) e^{S_1(Z)/\epsilon}$ is present. From the exponential asymptotics of turning-point problems, as Z is analytically continued along $Z > 0$, it is hence possible for this decaying mode to switch-on one of the oscillatory modes. This occurs across Stokes lines that originate from the turning points, Z_j , where the cubic (A.1) has a double root in S' :

$$Z_j = \left(\frac{2^2}{3^3 \beta^2} \right)^{1/p} e^{\pi i(1+2j)/p}, \quad j \in \mathbb{Z}, \quad (26)$$

with $p = 2[4 - 6/(n+1)]$ from (A.3). Notice that, while the number of turning points is possibly infinite (for p transcendental) the functions S'_1 , S'_2 , and S'_3 are smoothly varying in n . Above, only the turning points, Z_0 and Z_{-1} , are immediately relevant; all others produce Stokes lines that do not intersect $Z > 0$, or are on inaccessible Riemann sheets.

There are essentially two sets of relevant Stokes lines. First, the Stokes lines prescribed by

$$\text{Im} \left[\int_{Z_0}^Z (S'_1 - S'_3) dt \right] = 0 \quad \text{and} \quad \text{Re} \left[\int_{Z_0}^Z (S'_1 - S'_3) dt \right] \geq 0, \quad (27)$$

correspond to $\tilde{A}_1 e^{S_1/\epsilon}$ switching on $\tilde{A}_3 e^{S_3/\epsilon}$. Secondly, the Stokes lines prescribed by

$$\text{Im} \left[\int_{Z_{-1}}^Z (S'_1 - S'_2) dt \right] = 0 \quad \text{and} \quad \text{Re} \left[\int_{Z_{-1}}^Z (S'_1 - S'_2) dt \right] \geq 0, \quad (28)$$

correspond to $\tilde{A}_1 e^{S_1/\epsilon}$ switching on $\tilde{A}_2 e^{S_2/\epsilon}$. These two Stokes lines are complex-conjugate pairs, and indeed they intersect at a common point along $Z > 0$, and hence produce real-valued oscillatory terms on the real Z -axis. The key Stokes lines are now shown in Fig. 6 for the cases of $n = \{3, 2.5, 2, 1.7, 1.5\}$. These plots can be compared with Fig. 6 of [2]. Thus, we see that as n decreases from $n = 3$, the turning point Z_0 smoothly rotates anti-clockwise. The accompanied Stokes line geometry also shifts smoothly.

The remaining procedure is algebraically intensive, but can be explained concisely. By applying the formulae for Airy-type turning-point problems, the Stokes multipliers for the above switchings can be determined. This essentially establishes the form of $\tilde{A}_{2,3} e^{S_{2,3}/\epsilon}$. Then subsequent analysis as $Z \rightarrow 0$ allows the matching of these expressions to the generic form (20) applicable for $z = \mathcal{O}(1)$. In Appendix B, we present the key conclusion, which is that for z real, the localised oscillation is given by

$$\phi_{\text{exp}} \sim \left[\mathcal{O}(1) \text{ function of } z \text{ and } n \right] \epsilon^{-\tilde{\gamma}} \exp \left[-\frac{1}{\epsilon} \left(\tilde{\chi}(z; n) + i\beta \log \epsilon \right) \right] + \text{c.c.}, \quad (29)$$

where $\tilde{\chi}$ is related to (19), and $\tilde{\gamma}$ and β are functions of n . Above, we have separated the ϵ dependence and suppressed the constant pre-factor. This result is now used in the selection mechanism of Section 7 to generate the sequence (14).

6. Generation of the exponentials from the imaginary-axis singularities

We shall now see that when n is sufficiently small, additional singularities are introduced in ϕ_0 along the imaginary z -axis; these produce Stokes lines that intersect $z = 0$, and hence additional exponentially-small terms. Because the Stokes lines only occur along the imaginary axis, the additional terms cannot be switched off, and this ultimately leads to merging of the branches in the bifurcation diagram. In contrast to the far-field analysis of Section 5, the derivation of the exponentially-small terms in this section follows from the standard methodology of [1].

We return to the regular series expansion of ϕ in (15). When substituted into (10), the leading-order problem as $\epsilon \rightarrow 0$ satisfies

$$-\frac{d}{dz} (\phi_0^{2-n} \phi'_0) = -\alpha \phi_0 + \beta z \phi'_0, \quad (30a)$$

$$\phi'_0(0) = 0, \quad (30b)$$

$$\phi_0 \sim z^{\alpha/\beta}, \quad z \rightarrow \infty, \quad (30c)$$

with the final far-field condition applied along the real axis. The above system for ϕ_0 is then solved numerically, and it is subsequently confirmed that for $z \in \mathbb{R}$, solutions of the full problem in (10) are well approximated by ϕ_0 at small values of ϵ .

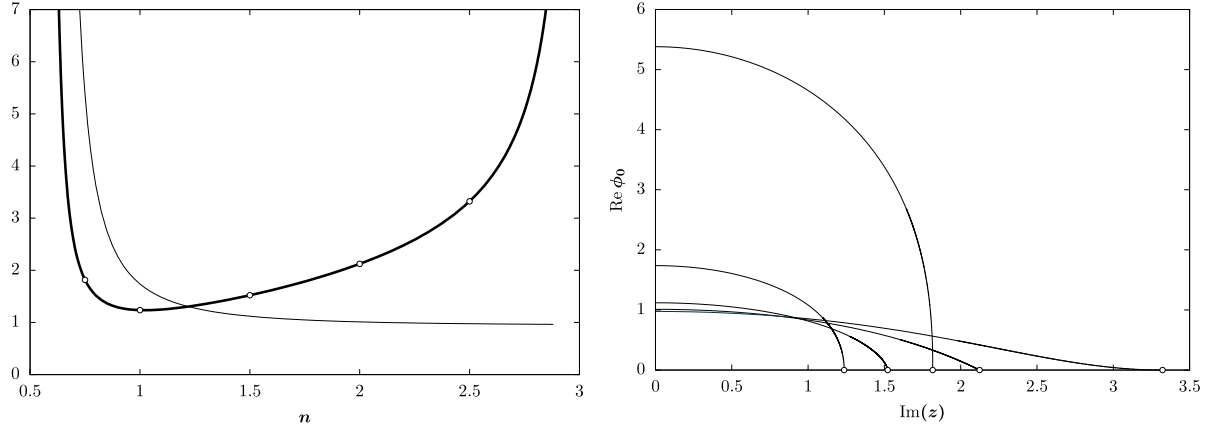


Fig. 7. Key properties of the leading-order solution $\phi_0(z)$. (Left) The value at the origin, $\phi_0(0)$ (thin) and the position of the branch point $z = \sigma_A$ (thick) on the imaginary axis over the range $1/2 < n < 3$. Open circles correspond to curves for $n = \{0.85, 1.0, 1.5, 2.0, 2.5\}$ shown to the right. (Right) Profiles for $\text{Re } \phi_0$ plotted along the imaginary axis.

Once ϕ_0 has been solved along the real z -axis from (30), the values of $\{\phi_0(0), \phi'_0(0)\}$ are known, and the differential equation (30a) can be solved as an initial-value problem to obtain $\phi_0(z)$ at any desired value of $z \in \mathbb{C}$. By exploring $z \in \mathbb{C}$, we detect for $n < 3$ a pair of singularities (branch points) on the imaginary axis at $z = \pm\sigma_A$ with $\text{Im } \sigma_A > 0$. Plots of $\text{Re } \phi_0$ on the imaginary axis are shown in Fig. 7 (right). A formal dominant-balance argument on (30a) can be applied in order to conclude that as $z \rightarrow \sigma_A$, the leading-order local structure of ϕ_0 at this branch point obeys

$$\phi_0(z) \sim c(z - \sigma_A)^{\frac{1}{3-n}}, \quad (31)$$

for $c \in \mathbb{C}$; this predicated behaviour agrees with the computed profiles shown in Fig. 7. Rather than the direct numerical fit shown in the figure, we may alternatively verify the nature of the singularity through a contour integration of ϕ'_0/ϕ_0 about σ_A . For $n = 2$, (30) is a linear problem that can be solved explicitly in terms of Kummer (hypergeometric) functions yielding $\phi_0(0) = \sqrt{3} \Gamma^2(2/3)/\pi$ and σ_A being a simple zero.

For a fixed point $z \in \mathbb{C}$, the singularity in (31) (and its complex conjugate, $-\sigma_A$), may have significant effects on the convergence properties of the asymptotic expansion (15). Note that at $\mathcal{O}(\epsilon^{2m})$ in (10a), under the substitution of (15), the determination of ϕ''_m must depend, in part, on ϕ'''_{m-1} . Thus, each subsequent order requires two derivatives of the previous order, and this has the effect of increasing the strength of any singularity present in the early terms. Although the full $\mathcal{O}(\epsilon^{2m})$ equation is prohibitively complicated due to the inherent nonlinearity of the original ODE, the late terms are nevertheless dominated by the above multiplicative effect. Consequently, the asymptotic expansion (15) can be shown to diverge in the limit $m \rightarrow \infty$. This divergence is a generic property of most singular differential equations (cf. [1,40]).

As presented in Section 4, in order to determine exponentially-small switchings found at optimal truncation, we require a characterisation of the divergence of ϕ_m as $m \rightarrow \infty$ [i.e. in order to study the remainder equation of (17a)]. Thus, we posit a factorial-over-power ansatz,

$$\phi_m(z) \sim \frac{A(z)\Gamma(2m + \gamma)}{[\chi(z)]^{2m + \gamma}} \quad \text{as } m \rightarrow \infty, \quad (32)$$

where $\gamma \in \mathbb{C}$ is constant, and χ and A are complex-valued functions to be determined. Here, the re-use of χ and A as

compared to (18) is intentional. We can now substitute the ansatz (32) into the $\mathcal{O}(\epsilon^{2m})$ equation derived from (10a) and derive the asymptotics as $m \rightarrow \infty$. The relevant terms at $\mathcal{O}(\epsilon^{2m})$ are

$$\begin{aligned} & \left[\phi_0^3 \phi'''_{m-1} + \phi_0^{2-n} \phi''_m \right] + \left[3\phi_0^2 \phi'_0 \phi'''_{m-1} + 2(2-n)\phi_0^{1-n} \phi'_0 \phi'_m \right. \\ & \left. + (2-n)\phi_0^{1-n} \phi_1 \phi''_{m-1} \right] = -\beta z \phi'_m + \dots \end{aligned} \quad (33)$$

Substitution of ansatz (32) then yields, at leading order as $m \rightarrow \infty$, a dominant balance between the first set of square bracketed terms in (33). This gives $\phi_0^3(\chi')^4 = -\phi_0^{2-n}(\chi')^2$, and hence [cf. (19)]

$$\chi(z) = \chi_A(z) = i \int_{\sigma_A}^z K(t) dt, \quad \text{with } K(t) = \frac{1}{[\phi_0(t)]^{(n+1)/2}}. \quad (34)$$

Above, the initial point of integration is chosen so that $\chi = 0$ at the chosen singularity, $z = \sigma_A$, forcing the divergence in (32). The positive square root branch is chosen so that $e^{-\chi_A/\epsilon}$ is exponentially small on the real axis. The similarity with the exponential argument in the generic WKB form of (18) is not coincidental, but rather due to the closeness of Eqs. (17) and (33). In addition, note that divergence is captured by a summation of terms of the form (32) due to each singularity in the analytic continuation of the early orders. In particular, we may include a similar χ due to $z = -\sigma_A$; by linearity, this can be considered separately and involves the negative of (34).

Not all singularities in the analytic continuation of ϕ_0 are of sufficient strength to cause divergence. In the limit $z \rightarrow \sigma_A$, it follows from (31) and (34) that

$$\chi_A(z) \sim \tilde{c}(z - \sigma_A)^{\frac{3}{2} \frac{5/3-n}{3-n}}. \quad (35)$$

where $\tilde{c} \in \mathbb{C}$. Consequently, the singularity at $z = \sigma_A$ (similarly $-\sigma_A$) is of sufficient strength to force divergence when $n < n^* = 5/3$. This is a key threshold for the presence of exponentially-small terms associated with $\pm\sigma_A$.

The other components of (32), namely A and γ , can also be computed in the usual way. We shall not need the prefactor, A , for the later discussion, but note that γ is calculated by requiring that the ansatz (32), matches the requisite scaling of ϕ_0 when $m = 0$ and $z \rightarrow \sigma_A$. Its value is given in (B.6).

We have thus completed the first task of the exponential asymptotic analysis, which is to characterise the divergence of (15) via the factorial-over-power expression (32). We may now

insert the late-term form (32) into the equation for the remainder, (17), and solve for the remainder of the optimally truncated series. This follows the basic procedures of optimal truncation and Stokes line smoothing below (cf. Berry [37,38], Chapman et al. [2]) but the final result is universal. It can be shown that when optimally truncating, the remainder can be written as (20) and the Stokes multiplier is given by $\mathcal{S}(z; \epsilon) = 2\pi i/\epsilon^\gamma$ (see e.g. Section 2 of [1], Section 4 of [41], or Section 2 of [42]). In addition, the terms (20) are switched on across Stokes lines given by Dingle's condition [43],

$$\text{Im } \chi(z) = 0 \quad \text{and} \quad \text{Re } \chi(z) \geq 0. \quad (36)$$

We thus consider the above condition applied to (34). The singular, χ_A , with the positive sign chosen indeed confirms that there exists a Stokes line down the imaginary axis $z = \sigma_A$. Similarly, there exists a Stokes line from $z = -\sigma_A$ up the imaginary axis when using the negative branch. All together, we expect the following switching from the imaginary-axis singularities:

$$\phi_A \sim \left[2\pi i A(z) \right] \epsilon^{-\gamma_A} e^{-\chi_A(z)/\epsilon} + \text{c.c.} \quad (37)$$

Above, $\gamma = \gamma_A$ is the constant that appears in the late terms of (32). The particular details of the prefactor, $2\pi i A(z)$, will be secondary in this paper, and we shall focus primarily on the exponential scaling, and the algebraic power of ϵ .

7. Selection mechanisms

We have presented the origins of two key exponentials. One from (29) scales as $e^{-\tilde{\chi}/\epsilon}$ and the other from (37) scales as $e^{-\chi_A/\epsilon}$. When z is real, let us write the real and imaginary parts of the exponential arguments as

$$\tilde{\chi}(z; n) = L_1(n) - iW_1(z; n), \quad (38a)$$

$$\chi_A(z; n) = L_2(n) - iW_2(z; n). \quad (38b)$$

The formula for $\tilde{\chi}$ is given in (B.2) while the formula for χ_A is given in (34). Notice that both these functions have constant real parts on $z \in \mathbb{R}$ due to the reality of ϕ_0 on the axis [cf. the formulae in (B.8)].

Therefore, there exists two situations depending on whether the disjoining parameter, n , is greater-than or less-than $n^* = 5/3$. If $n > n^*$, then as we had noted, an oscillation switches on as the solution is analytically continued from large positive z to the origin. From (29), this term behaves as

$$\begin{aligned} \phi_{\text{exp}} \sim & \left| (\mathcal{O}(1) \text{ function of } z \text{ and } n) \right| \epsilon^{-\tilde{\gamma}} \\ & \times \exp \left[-\frac{L_1(n)}{\epsilon} \right] \cos \left(\frac{W_1(z; n) - \beta \log \epsilon}{\epsilon} + \psi_1(z; n) \right). \end{aligned} \quad (39)$$

The quantities L_1 and W_1 , in addition to $\tilde{\gamma}$ and ψ_1 are explained in more detail in Appendix B. If the domain $z < 0$ is also considered, then a similar switching to (39) occurs upon passing the Stokes lines along the negative real axis. Then, if the parameter $\epsilon = \epsilon_m$ is chosen correctly, the oscillation is properly localised and the far-field boundary condition is satisfied to leading order in the exponential asymptotics. This localisation property is equivalent to requiring that the oscillation (39) satisfies a symmetry condition at the origin, or $\phi'_{\text{exp}}(0) = 0$. Then, differentiating (39) and setting the sinusoidal argument to zero, we require the leading-order selection condition:

$$\frac{W_1(z=0; n) - \beta \log \epsilon_m}{\epsilon_m} + \psi_1(z=0; n) = m\pi. \quad (40)$$

for $m \in \mathbb{Z}$. In the next section, we provide more details on how (40) can be verified.

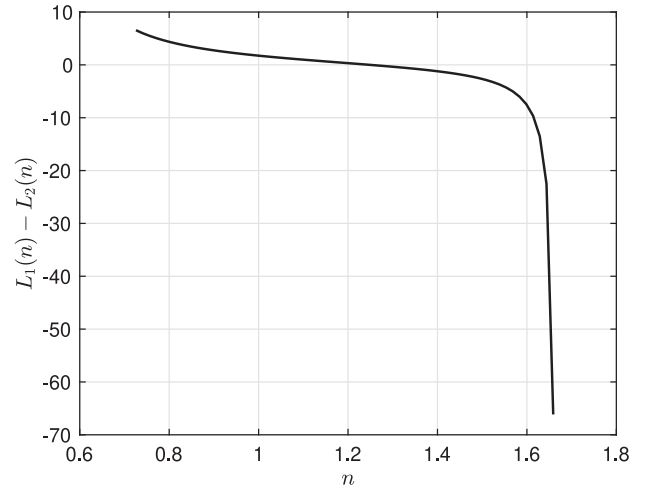


Fig. 8. A plot of the difference $L_1(n) - L_2(n) = \text{Re}(\tilde{\chi} - \chi_A)$ versus n , computed from (B.8). Note that as $n \rightarrow n^* = 5/3 \approx 1.67$ on the left, the exponential $e^{-L_2/\epsilon}$ is exponentially suppressed. However, for sufficiently small n , the dominance switches. The zero of the curve lies approximately at 1.25.

For $n < n^* = 5/3$, an additional Stokes line appears along the imaginary axis. As illustrated in Fig. 5(b), across the Stokes lines from $\pm\sigma_A$, a similar oscillation switches on, given by (37), or

$$\begin{aligned} \phi_A \sim & \left| (\mathcal{O}(1) \text{ function of } z \text{ and } n) \right| \epsilon^{-\gamma_A} \\ & \times \exp \left[-\frac{L_2(n)}{\epsilon} \right] \cos \left(\frac{W_2(z; n)}{\epsilon} + \psi_2(z; n) \right). \end{aligned} \quad (41)$$

Because there is only a central Stokes line, there is no switch-off of the oscillation, and (41) must necessarily be present in the far field. We may compare the exponential magnitudes, $e^{-L_1/\epsilon}$ and $e^{-L_2/\epsilon}$, via the difference, $L_1 - L_2$ is shown in Fig. 8. We see that near $n = 5/3$, where the exponential (41) is introduced, it is exponentially subdominant to (39). However, for n less than ≈ 1.25 , (41) dominates and hence solutions are not expected to exist for $\epsilon \rightarrow 0$.

When considering the half-domain $z > 0$, we apply a selection condition determined by both contributions, i.e.

$$\frac{d}{dz} (\phi_{\text{exp}}(z; n, \epsilon) + \frac{1}{2} \phi_A(z; n, \epsilon)) \Big|_{z=0} = 0. \quad (42)$$

which is the first-derivative symmetry condition applied to the exponentially-small terms, but now accounting for half the central contribution of ϕ_A since only half the Stokes line is crossed.

We may then insert (39) and (41) into (42) to see that the selection is governed by

$$\begin{aligned} |\tilde{F}(n)| \epsilon^{-\tilde{\gamma} + \gamma_A} \sin \left(\frac{W_1(0; n) - \beta \log \epsilon}{\epsilon} + \psi_1(0; n) \right) \\ + \exp \left\{ \frac{L_1(n) - L_2(n)}{\epsilon} \right\} = 0. \end{aligned} \quad (43)$$

Above, we have used the fact that $W_2(z=0; n) = 0$, associated with the fact that χ_A is purely real along the Stokes line running parallel to the imaginary axis. The pre-factor, $|\tilde{F}(n)|$, has been introduced to describe the general multiplier. At least in a symbolic form, (43) is the key result. When $n > n^*$, the second term can be ignored, and hence we recover (40). However, when $n < n^*$, the second term is included; as $n \rightarrow n^*$ on the left, this effect tends to zero, but for sufficiently small n (less than approximately 1.25),

Table 1

A table of $\Delta U_m/\pi$ values. From (45), we expect that as $m \rightarrow \infty$, $\Delta U_m/\pi \rightarrow 1$. The data is shown for values of n from 1.75 to 4.5, and for those seven differences, $\Delta U_m/\pi$, for which we possess numerical solutions (corresponding to the eight branches shown in Fig. 4).

n	$\Delta U_2/\pi$	$\Delta U_3/\pi$	$\Delta U_4/\pi$	$\Delta U_5/\pi$	$\Delta U_6/\pi$	$\Delta U_7/\pi$	$\Delta U_8/\pi$
1.75	0.9106	0.9289	0.9455	0.9593	0.9680	0.9757	0.9811
2.00	0.9188	0.9348	0.9493	0.9616	0.9706	0.9789	0.9847
2.25	0.9097	0.9309	0.9466	0.9592	0.9694	0.9782	0.9850
2.50	0.9031	0.9274	0.9438	0.9570	0.9675	0.9768	0.9845
2.75	0.8998	0.9255	0.9420	0.9554	0.9664	0.9758	0.9841
3.00	0.8995	0.9253	0.9420	0.9554	0.9666	0.9761	0.9846
3.25	0.9009	0.9265	0.9430	0.9563	0.9676	0.9772	0.9858
3.50	0.9018	0.9270	0.9433	0.9567	0.9679	0.9776	0.9861
3.75	0.9022	0.9269	0.9432	0.9564	0.9676	0.9774	0.9859
4.00	0.9024	0.9267	0.9427	0.9559	0.9671	0.9769	0.9855
4.25	0.9024	0.9262	0.9421	0.9552	0.9664	0.9762	0.9848
4.50	0.9022	0.9256	0.9413	0.9544	0.9656	0.9754	0.9840

the dominance switches with $L_1(n) - L_2(n) > 0$ and no solution of (40) as $\epsilon \rightarrow 0$. Hence the merging of branches.

8. Comparison of numerical and asymptotic results

It is possible to use the results (40) and (42) to generate the bifurcation curves of n vs $\epsilon_m(n)$. However, in practice this is quite an involved process since many of the components involved in the formulae require extensive derivations, similar to the prior analysis of $n = 3$ in the work of Chapman et al. [2]. Here, we shall devise a simple check of the selection condition (40). We proceed in a 'hybrid' fashion, combining some of the asymptotic structures derived previously with some minimal fitting; this bypasses the need to compute all the associated components of analysis, but nevertheless demonstrates key aspects.

Let us define the quantity

$$U(n, \epsilon) \equiv \frac{W_1(0; n) - \beta(n) \log \epsilon}{\epsilon}, \quad (44)$$

where W_1 is defined in (38a). By (40), it is then expected that for $n > 5/3$, adjacent eigenvalues, ϵ_m , obey

$$\frac{\Delta U_m}{\pi} \equiv \frac{U(n, \epsilon_m) - U(n, \epsilon_{m-1})}{\pi} \rightarrow 1 \quad \text{as } m \rightarrow \infty. \quad (45)$$

We have constructed Table 1, which concerns the twelve values of the parameter $n = \{1.75, 2.0, 2.25, \dots, 4.5\}$. For each value of n , we calculate $\Delta U_m/\pi$ using U from (44) for $m = 1, 2, 3, \dots, 7$. Values of ϵ_m are taken from the results of the full numerical computations (Fig. 4), while $W_1(0; n)$ is calculated directly from (38a). Even for the relatively small values of m that we use (the first eight branches), the table confirms the asymptotic trend (45), with all rows appearing to rapidly asymptote to one.

We now seek to generate a bifurcation diagram, which includes both regions of $n > 5/3$ and $n < 5/3$. When $n > 5/3$, the bifurcation diagram can be generated by applying a numerical root finder on (40) to determine the branches $\epsilon = \epsilon_m$. Similarly, for $n < 5/3$, we solve (43) numerically. Formulae for $\tilde{\gamma}$, γ_A , L_1 , L_2 , and W_1 are presented in Appendix B. The generation of the bifurcation diagram is complicated by virtue of the difficulty of calculating the numerical prefactor, $|\tilde{F}(n)|$ and phase shift $\Psi_1(0; n)$, which are quite convoluted components to obtain in the asymptotic analysis.

We fit the value of $\Psi_1(0; n)$ in the following way. Note from (40) and (44) that $U(n, \epsilon_m) + \Psi_1(0; n) = m\pi$. For $n > 5/3$, we

shall fit $\Psi_1(0; n)$ by using the data for the $m = 8$ th family. That is, for each given n value, we use

$$\Psi_1(0; n) \approx 8\pi - U(n, \epsilon_8(n)), \quad (46)$$

where $\epsilon_8(n)$ is given by the full numerical solution (i.e. one of the curves shown in Fig. 4). For $n < 5/3$, the linearly extrapolated value of Ψ_1 , via (46) is used. The other quantity that is unknown is $|\tilde{F}(n)|$. For this, we choose a simple value: $|\tilde{F}(n)| = 10$. In essence, different choices for $|\tilde{F}|$ will alter the location of the turning points of the bifurcation diagrams. The choice $|\tilde{F}(n)| = 10$ is an approximate value so that the $m = 2$ branch has a turning point that matches the asymptotics to visual accuracy; other choices of $|\tilde{F}|$ ranging from 1 to 1000 (say) has only a minor effect on the final curves near the turning points. More sophisticated fitting choices can be taken, but the choice above is sufficient to illustrate the general trends.

The result is shown in Fig. 9. We observe a good match between asymptotics and the exact numerical solutions, even at relatively large values of ϵ ; the fit is expected to improve for smaller values of ϵ . The agreement for the largest branch of ϵ -values is poor, but this is likely a function of our method of fitting the asymptotic components, where we have used the expected behaviour in the $\epsilon \ll 1$ regime.

9. Open questions on the effect of quartet singularities

In the analysis of the $n = 3$ by [2], it was noted that there exists an intricate structure of singularities consisting of poles arranged in a periodic array in the four quadrants. In the first quadrant, the singularities tend to infinity along the angle of $\text{Arg}(z) = \beta\pi/2$ with $\beta = 2/5$. Then each such singularity, say at $z = \sigma_j$, is contained in the set $\{\sigma_j, -\sigma_j, \bar{\sigma}_j, -\bar{\sigma}_j\}$ for $j = 1, 2, 3, \dots$. We shall call these the 'quartet singularities'. For general values of n , there is a similarly intricate structure shown in Fig. 10. A dominant balance argument indicates that such points can be of zero-type or pole-type, and will exhibit scaling laws of $\mathcal{O}(z - \sigma_j)^{1/(3-n)}$ or $\mathcal{O}(z - \sigma_j)^{1/(2-n)}$ respectively. The analysis of the movement and properties of these singularities as n varies seems highly non-trivial—both analytically and numerically.

Typically, in an exponential asymptotic analysis, the nearest singularities to the domain of consideration (here, $z \in \mathbb{R}$) dominate, and hence only their corresponding Stokes lines need to be considered at leading order. However, the $n = 3$ case

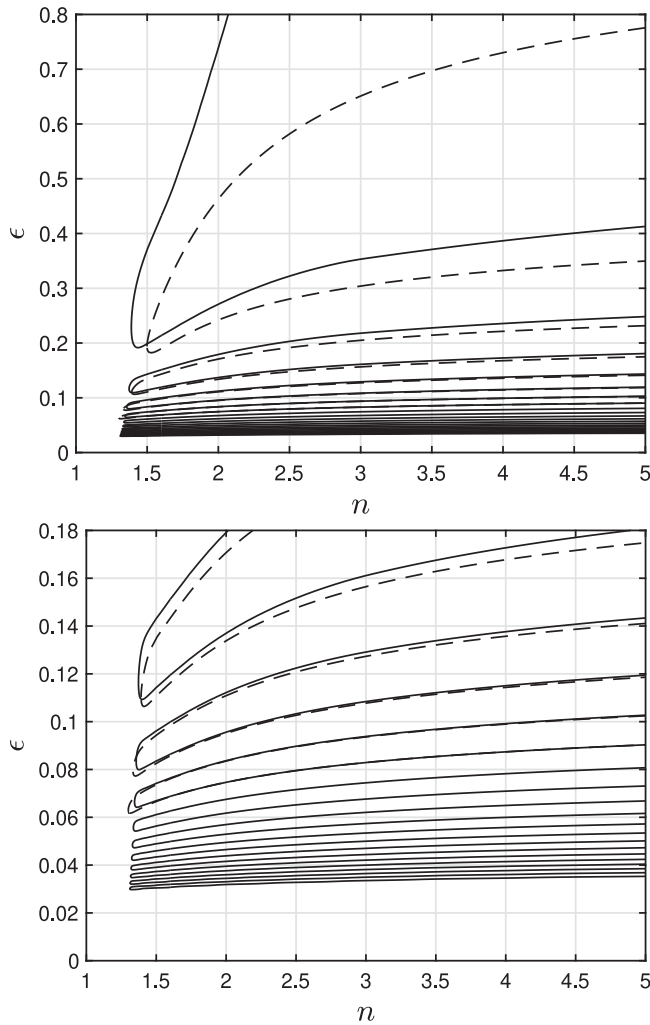


Fig. 9. (Top) A bifurcation diagram showing the selected values of ϵ versus the generalised rupturing parameter, n . The numerical solutions of the first $m = 8$ branches, computed from the differential equation, are shown dashed (cf. Fig. 4). Solid curves denote the asymptotic predictions; for $n < 5/3$, these are computed using (43) and for $n > 5/3$, these are computed using (40). Additional asymptotic predictions, beyond the $m = 8$ branch, are included. (Bottom) An enlargement showing the additional asymptotic predictions for smaller $\epsilon = \epsilon_m$ branches.

exhibits a peculiarity in which the contributions of the form (20) increase in size for each subsequent singularity extending to infinity. This then motivates the far-field analysis of Section 5 where the largest exponential for $z \gg 1$ is considered. In [2], an argument was given for why the Stokes line structure for such quartet singularities is dominated by the far-field contribution (29).

We believe that for general n , the same arguments presented for $n = 3$ hold. However, an open question is whether the selection law (43) must be appropriately modified to include such quartet contributions. This seems to be an extremely challenging problem, since extensive statistics of the singularities must be generated for each n , but accurate numerics of the analytic continuation problem are difficult to obtain for large values of $|z|$.

There are further intuitive reasons to believe that these quartet singularities can be neglected. Firstly, the numerical fit shown in Fig. 9 demonstrates good agreement to the primary features of the exact eigenvalues. Secondly, in the case of $n = 2$, the

equation for ϕ_0 in (30a) is linear, and the analytic continuation exhibits no singularities, except for $|z| \rightarrow \infty$. Hence, in this case, it is clear that the exponential asymptotics is exclusively determined by the far-field analysis of Section 5 where $n = 2$ is clearly unexceptional. The bifurcation diagram confirms indeed that $n = 2$ is an unexceptional point, and this lends further confidence that within a neighbourhood of this point, the quartet effects can be neglected.

10. Discussion

Intriguingly, the generalised rupture problem that forms the subject of this work presents a somewhat pathological study in exponential asymptotics—for reasons that we believe are secondary to the main message. These reasons seem to relate to the form of the nonlinearity and the scalings associated with the governing ODE (Appendix A). As noted earlier, a complete presentation of the full mathematical details will follow in a forthcoming effort; such details are important in the technical sense, but we believe that an exhaustive presentation would detract from the key ideas here.

A concise summary is as follows. The generalised rupture problem is a prototypical example in nonlinear dynamics where startling complex behaviours emerge when considering the existence of self-similar solutions as a function of an associated parameter (here, n , the disjoining parameter). As has been well known, when the classic case of $n = 3$ is chosen, an infinite and countably discrete set of similarity solutions (branches) emerges. However, when n is varied, it is possible for such branches to merge, and then annihilate. Prior to this work, it had not been clear how this behaviour can be predicted analytically.

Here, we have shown that it is possible to understand this phenomenon via exponential asymptotics when the large-branch limit is taken. Specifically, when the parameter n is sufficiently large, solutions exhibit localised oscillations, from which a matching condition dictates the selection process. However, when n is sufficiently small, the appearance of additional singularities in the complex plane forces the emergence of further unmatchable contributions—hence no solutions are formally possible. As a first approximation, we have further predicted that this threshold appears at $n = 5/3$.

There are several other examples from engineering and physics characterised by transition to discrete self-similarity leading to iterated structures, but for which there is no theory. For example, numerical simulations of the frictional dynamics of two elastic bodies in contact reveals a series of bifurcations on the branch of self-similar steady states [44].

Iterated structures can be viewed as an example of emergence and self-organisation, ultimately responsible for the dynamic and adaptive increase in order and structure without external direction, manipulation or control: a certain pattern is born; then a new pattern evolves based on that pattern, and this process will recur many times. Such phenomena are often present in complex dynamical systems, and play a central role in nonlinear dynamics. In such systems the level of complexity is such that it is impossible to impose a structure *a priori*: the systems need to self-organise via a one-way formation of macroscopic order from micro-dynamics. At the same time, the large number of micro-level elements imposes a need for emergence via the circulation of information from the macro- to the micro-level, and vice versa.

The framework outlined here offers a promising approach not only to understand the emergence-creating mechanism in nonlinear systems with self-similar behaviour, but also to inform future studies on how to control pattern dynamics: what condition(s) should be imposed on the micro-/macro-level in order to facilitate the successive evolution of certain pattern-generating systems.

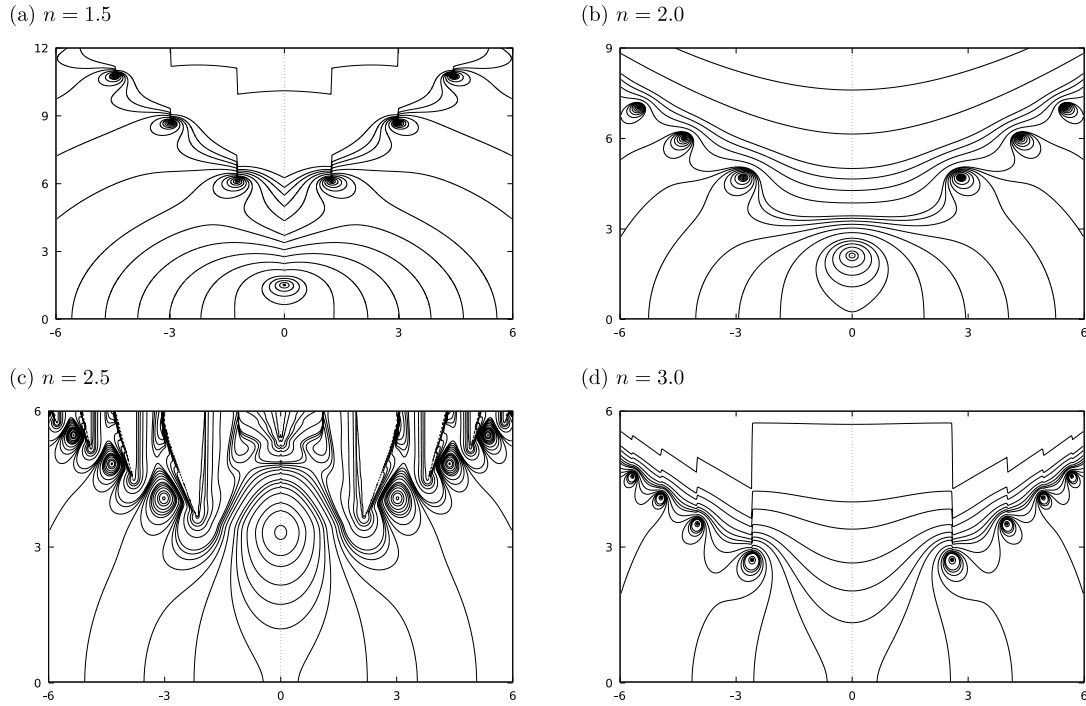


Fig. 10. Contour plots of $|\phi_0(z)|$ in the upper half z -plane at $n = \{1.5, 2, 2.5, 3\}$. Notice the critical points on the imaginary axis for $n = \{1.5, 2.0\}$, and the pattern of quartet branch points for $n = \{1.5, 2.5, 3.0\}$. For $n = 2$, ϕ_0 is the solution of a linear PDE and the pattern of points seen in the contour plots correspond to simple zeros.

CRediT authorship contribution statement

S. Jonathan Chapman: Conceived and designed the analysis, Contributed data or analysis tools, Performed the analysis, Wrote the paper. **Michael C. Dallaston:** Conceived and designed the analysis, Contributed data or analysis tools, Performed the analysis, Wrote the paper. **Serafim Kalliadasis:** Conceived and designed the analysis, Contributed data or analysis tools, Performed the analysis, Wrote the paper. **Philippe H. Trinh:** Conceived and designed the analysis, Contributed data or analysis tools, Performed the analysis, Wrote the paper. **Thomas P. Witelski:** Conceived and designed the analysis, Contributed data or analysis tools, Performed the analysis, Wrote the paper.

Declaration of competing interest

The authors declare that they have no known competing financial interests or personal relationships that could have appeared to influence the work reported in this paper.

Data availability

No data was used for the research described in the article.

Acknowledgements

The authors would like to thank the Isaac Newton Institute for Mathematical Sciences for support and hospitality during the programme Applicable Resurgent Asymptotics when work on this paper was undertaken. This work was supported by EPSRC, United Kingdom Grant No. EP/R014604/1. PHT gratefully acknowledges support from EPSRC, United Kingdom Grant No. EP/V012479/1 and also Lincoln College (Oxford), United Kingdom and the support of the Zilkha Fund. SK acknowledges support

from EPSRC, United Kingdom Grants No. EP/K008595/1 and No. EP/L020564/1, and ERC, via Advanced Grant No. 247031.

Appendix A. Additional details of the far-field scaling

For general n , the far-field analysis of Section 5 parallels the analysis done for the special case of $n = 3$ in Section 6 of [2]. In fact, the methodology presented in the former work is generalised in a straightforward fashion.

Substituting the WKBJ ansatz (24) into (23) yields an equation for $S'(Z)$,

$$Z^2(S')^3 + S' + \beta Z^{\hat{c}+1} = 0 \quad \text{with} \quad \hat{c} \equiv 3 - \frac{6}{n+1}. \quad (\text{A.1})$$

Then, from the cubic equation, it follows that the three roots are given by

$$S'_1 = -\left(\frac{2}{3\beta}\right)^{1/3} \frac{1}{B^{1/3}} + \left(\frac{\beta}{2 \cdot 9}\right)^{1/3} \frac{B^{1/3}}{Z^2}, \quad (\text{A.2a})$$

$$S'_{2,3} = \left(\frac{2}{3\beta}\right)^{1/3} \left(\frac{1}{2} \pm \frac{\sqrt{3}}{2}i\right) \frac{1}{B^{1/3}} - \left(\frac{\beta}{2 \cdot 9}\right)^{1/3} \left(\frac{1}{2} \mp \frac{\sqrt{3}}{2}i\right) \frac{B^{1/3}}{Z^2}, \quad (\text{A.2b})$$

where we have defined

$$B \equiv -9Z^{4+\hat{c}} + 9Z^3 \sqrt{Z^p + \frac{4}{26\beta^2}} \quad \text{and} \quad p \equiv 2(\hat{c} + 1) = 2\left(4 - \frac{6}{n+1}\right). \quad (\text{A.3})$$

Note that there are turning points where the cubic (A.1) has a double root for S' . These are given in (26). For the purpose of this work, the main utility of the above is the use of quantities $S_{1,3}$, found in the formulae of Appendix B.

Appendix B. Formulae of exponentially-small switchings

We have noted in Section 5 that the far-field methodology adjusts the switching to be

$$\phi_{\text{exp}} \sim \left[\mathcal{O}(1) \text{ function of } z \text{ and } n \right] \epsilon^{-\tilde{\gamma}} \times \exp \left[-\frac{1}{\epsilon} \left(\tilde{\chi}(z; n) + i\beta \log \epsilon \right) \right] + \text{c.c.} \quad (\text{B.1})$$

For the purpose of the comparison in Section 8, we are interested in the algebraic scaling, $\epsilon^{-\tilde{\gamma}}$, and the exponential scalings on the magnitude and phase. The following formulae are found by essentially following the procedure in Appendix A of [2], but with general values of n . Following the far-field asymptotic analysis, we establish that the exponential argument given in (B.1) is

$$\tilde{\chi}(z; n) = i \int_s^z K(t; n) dt - b(n), \quad (\text{B.2})$$

where $K(t; n) = [\phi_0(t)]^{-(n+1)/2}$ is given in (19) and b is defined by

$$b(n) \equiv i \log \left(\frac{Z_0}{s} \right) + i \int_s^\infty \left(K(t; n) - \frac{1}{t} \right) dt + \int_{Z_0}^0 \left(S'_3(t; n) - S'_1(t; n) + \frac{i}{t} \right) dt. \quad (\text{B.3})$$

In the above formulae, the S_k functions are calculated from (A.2) and Z_0 is the first ($j = 0$) turning point from (26). In addition, s , appearing in both (B.2) and (B.3) is an arbitrary constant which can be chosen to be $s = 1$ for simplicity (its value changes the prefactor multiplier in (B.1)). The formula (B.3) can be compared with eqn (A.19) in [2] for the case of $n = 3$.

The value of $\tilde{\gamma}$ follows from a complicated matching argument between $z = \mathcal{O}(1)$ and $Z = \mathcal{O}(1)$ regions. It is given by

$$\tilde{\gamma} = -\frac{-51 + 76n - 11n^2}{4(1 - 2n)^2}. \quad (\text{B.4})$$

For $n < n^* = 5/3$, the central Stokes lines produce a leading contribution given by (41). This time, however, the formulae are much simpler and are given by the universal form (37),

$$\phi_A \sim \left[\mathcal{O}(1) \text{ function of } z \text{ and } n \right] \epsilon^{-\gamma_A} \exp \left[-\frac{1}{\epsilon} \chi_A(z; n) \right] + \text{c.c.} \quad (\text{B.5})$$

The formula for χ_A is given in (34). The constant γ_A follows from a standard argument in exponential asymptotics where the late-order ansatz (32) is verified to be consistent with the singular behaviour of ϕ_0 as $z \rightarrow \sigma_A$. We find that

$$\gamma_A = \frac{3 + n}{2(5 - 3n)}. \quad (\text{B.6})$$

Note that in the main text, we have written the real and imaginary parts of the singular functions as

$$\tilde{\chi}(z; n) = L_1(n) - iW_1(z; n), \quad (\text{B.7a})$$

$$\chi_A(z; n) = L_2(n) - iW_2(z; n). \quad (\text{B.7b})$$

When z is real, the associated components can be simplified. For instance, we use (B.2) and (B.3) with $s = 1$, and (34) to write

$$L_1(n) = -\text{Re } b(n) = -\text{Re} \left[i \log Z_0 + \int_{Z_0}^0 \left(S'_3(t; n) - S'_1(t; n) + \frac{i}{t} \right) dt \right], \quad (\text{B.8a})$$

$$L_2(n) = \text{Re } \chi_A = \text{Re} \left[i \int_{\sigma_A}^0 \frac{1}{[\phi_0(t)]^{(n+1)/2}} dt \right]. \quad (\text{B.8b})$$

The second formula above uses the fact that χ_A has constant real part on the real z -axis.

B.1. Selection condition for $n = 3$

For consistency, let us verify the case of $n = 3$, which was the core subject of [2]. We set $z = 0$ and evaluate $W_1 = -\text{Im } \tilde{\chi}$ from (B.2) and (B.7a) with $s = 1$. With $K = 1/\phi_0^2$, the result is that

$$W_1(z = 0; n = 3) = -\int_1^0 \frac{1}{[\phi_0(t)]^2} dt + \text{Im } b, \quad (\text{B.9})$$

where we have used the fact that $\phi_0(t)$ is real on the real t -axis. Next, from (B.3), we have

$$b = i \log(Z_0) + i \int_1^\infty \left(\frac{1}{\phi_0^2} - \frac{1}{t} \right) dt + \int_{Z_0}^0 \left(S'_3 - S'_1 + \frac{i}{t} \right) dt, \quad (\text{B.10})$$

and $Z_0 = (25/27)^{1/5} e^{\pi i/5}$ follows from (26). We then see that (B.10) matches formula (A.19) of [2].

Moreover, let us examine the exponential (39) when evaluated at the origin, $z = 0$. Using the above, the cosine factor in (39) is given by

$$\cos \left(-\frac{1}{\epsilon} \int_1^0 \frac{1}{\phi_0^2} dt + \frac{\text{Im } b}{\epsilon} - \frac{2 \log \epsilon}{5\epsilon} + \psi_1 \right), \quad (\text{B.11})$$

while from (B.4), $\tilde{\gamma} = -39/50$, which now matches the corresponding entry in eqn (6.16) of [2]. The computation of W_1 in Section 8 for the general n values is done analogously.

References

- [1] S.J. Chapman, J.R. King, K.L. Adams, Exponential asymptotics and Stokes lines in nonlinear ordinary differential equations, *Proc. R. Soc. Lond. Ser. A Math. Phys. Eng. Sci.* 454 (1998) 2733–2755.
- [2] S.J. Chapman, P.H. Trinh, T.P. Witelski, Exponential asymptotics for thin film rupture, *SIAM J. Appl. Math.* 73 (1) (2013) 232–253.
- [3] W. Zhang, J. Lister, Similarity solutions for van der Waals rupture of a thin film on a solid substrate, *Phys. Fluids* 9 (1999) 2454–2462.
- [4] T.P. Witelski, A. Bernoff, Stability of self-similar solutions for van der Waals driven thin film rupture, *Phys. Fluids* 11 (9) (1999) 2443–2445.
- [5] B.B. Mandelbrot, *The Fractal Geometry of Nature*, MacMillan, London, 1983.
- [6] M. Choptuik, Universality and scaling in gravitational collapse of a massless scalar field, *Phys. Rev. Lett.* 70 (1993) 9–12.
- [7] A. Pumir, E. Siggia, Development of singular solutions to the axisymmetric euler equations, *Phys. Fluids* 4 (1992) 1472–1491.
- [8] M.C. Dallaston, D. Tseluiko, Z. Zheng, M.A. Fontelos, S. Kalliadasis, Self-similar finite-time singularity formation in degenerate parabolic equations arising in thin-film flows, *Nonlinearity* 30 (7) (2017) 2647.
- [9] M.C. Dallaston, M.A. Fontelos, D. Tseluiko, S. Kalliadasis, Discrete self-similarity in interfacial hydrodynamics and the formation of iterated structures, *Phys. Rev. Lett.* 120 (3) (2018) 034505.
- [10] R. Combescot, M. Ben Amar, Selection of Saffman–Taylor fingers in the sector geometry, *Phys. Rev. Lett.* 67 (1991) 453–456.
- [11] M. Ben Amar, V. Hakim, M. Mashaal, Y. Couder, Self-dilating viscous fingers in wedge-shaped Hele–Shaw cells, *Phys. Fluids A* 3 (1991) 1687–1690.
- [12] C.M. Bender, S. Boettcher, Real spectra in non-Hermitian Hamiltonians having PT symmetry, *Phys. Rev. Lett.* 80 (1998) 5243–5246.
- [13] S.J. Chapman, P.H. Trinh, Exponential asymptotics for the eigenvalues in the broken PT-symmetric region, 2019, arXiv:1906.08218.
- [14] K. Deng, H. Levine, The role of critical exponents in blow-up theorems: the sequel, *J. Math. Anal. Appl.* 243 (2000) 85–126.
- [15] S. Kalliadasis, C. Ruyer-Quil, B. Scheid, M.G. Velarde, *Falling Liquid Films*, in: Springer Series on Applied Mathematical Sciences, vol. 176, Springer, London, 2012.
- [16] L. Morrow, T. Moroney, M.C. Dallaston, S. McCue, A review of one-phase Hele–Shaw flows and a level-set method for non-standard configurations, *The ANZIAM J.* 63 (3) (2021) 269–307.
- [17] R. Meyer, Exponential asymptotics, *SIAM Rev.* 22 (1980) 213–224.
- [18] J.R. King, S.J. Chapman, Asymptotics beyond all orders and Stokes lines in nonlinear differential-difference equations, *Eur. J. Appl. Math.* 12 (4) (2001) 433–463.
- [19] R. Combescot, Saffman–Taylor fingers in the sector geometry, *Phys. Rev. A* 45 (1992) 873–884.
- [20] S. Tanveer, Analytic theory for the selection of Saffman–Taylor fingers in the presence of thin film effects, *Proc. R. Soc. Lond. Ser. A Math. Phys. Eng. Sci.* 428 (1875) (1990) 511–545.

- [21] S.J. Chapman, On the role of Stokes lines in the selection of Saffman–Taylor fingers with small surface tension, *Eur. J. Appl. Math.* 10 (6) (1999) 513–534.
- [22] J. Shelton, P. Milewski, P.H. Trinh, On the structure of steady parasitic gravity-capillary waves in the small surface tension limit, *J. Fluid Mech.* 922 (2021) A16.
- [23] J. Shelton, P.H. Trinh, Exponential asymptotics for steady parasitic capillary ripples on steep gravity waves, *J. Fluid Mech.* 939 (2022) A17.
- [24] S.J. Chapman, G. Kozyreff, Exponential asymptotics of localised patterns and snaking bifurcation diagrams, *Physica D* 238 (3) (2009) 319–354.
- [25] S.J. Chapman, B.J. Hunton, J.R. Ockendon, Vortices and boundaries, *Quart. J. Appl. Math.* 56 (1998) 507–5129.
- [26] M.C. Dallaston, M.A. Fontelos, M.A. Herrada, J.M. Lopez-Herrera, J. Eggers, Regular and complex singularities of the generalized thin film equation in two dimensions, *J. Fluid Mech.* 917 (2021) A20.
- [27] A. Oron, S.H. Davis, S.G. Bankoff, Long-scale evolution of thin liquid films, *Rev. Modern Phys.* 69 (1997) 931–980.
- [28] T. Myers, Thin films with high surface tension, *SIAM Rev.* 40 (1998) 441–462.
- [29] R.V. Craster, O.K. Matar, Dynamics and stability of thin liquid films, *Rev. Modern Phys.* 81 (2009) 1131–1198.
- [30] G.F. Teletzke, H. Ted Davis, L.E. Scriven, How liquids spread on solids, *Chem. Eng. Commun.* 55 (1–6) (1987) 41–82.
- [31] W. Boos, A. Thess, Cascade of structures in long-wavelength Marangoni instability, *Phys. Fluids* 11 (1999) 1484–1494.
- [32] S. Shklyaev, A. Straube, A. Pikovsky, Superexponential droplet fractalization as a hierarchical formation of dissipative compactons, *Phys. Rev. E* 82 (2010) 020601:1–4.
- [33] S.G. Yiantsios, B.G. Higgins, Rayleigh–Taylor instability in thin viscous films, *Phys. Fluids A* 1 (1989) 1484–1501.
- [34] J.P. Burelbach, S.G. Bankoff, S.H. Davis, Nonlinear stability of evaporating/condensing liquid films, *J. Fluid Mech.* 195 (1988) 463–494.
- [35] D. Tseluiko, J. Baxter, U. Thiele, A homotopy continuation approach for analysing finite-time singularities in thin liquid films, *IMA J. Appl. Math.* 78 (4) (2013) 762–776.
- [36] C.M. Bender, S.A. Orszag, *Advanced Mathematical Methods for Scientists and Engineers*, McGraw-Hill, Inc., 1978.
- [37] M.V. Berry, Uniform asymptotic smoothing of Stokes discontinuities, *Proc. R. Soc. Lond. Ser. A* 422 (1989) 7–21.
- [38] M.V. Berry, Stokes’ phenomenon; smoothing a victorian discontinuity, *Publ. Math. Inst. Hautes Études Sci.* 68 (1989) 211–221.
- [39] R.B. White, *Asymptotic Analysis of Differential Equations*, World Scientific, 2010.
- [40] J.P. Boyd, The devil’s invention: Asymptotic, superasymptotic and hyperasymptotic series, *Acta Appl. Math.* 56 (1) (1999) 1–98.
- [41] S.J. Chapman, J.-M. Vanden-Broeck, Exponential asymptotics and gravity waves, *J. Fluid Mech.* 567 (2006) 299.
- [42] S. Crew, P.H. Trinh, Resurgent aspects of applied exponential asymptotics, 2023, arXiv:2208.07290.
- [43] R.B. Dingle, *Asymptotic Expansions: Their Derivation and Interpretation*, Academic Press, 1973.
- [44] R.C. Viesca, Self-similar slip instability on the interfaces with rate- and state-dependent friction, *Proc. R. Soc. Lond. Ser. A Math. Phys. Eng. Sci.* 472 (2016) 20160254.